JACS
JOURNAL OF THE AMERICAN CHEMICAL SOCIETY

ARTICLE

pubs.acs.org/JACS

High-Pressure in Situ ^{129}Xe NMR Spectroscopy and Computer Simulations of Breathing Transitions in the Metal−Organic Framework $Ni_2(2,6\text{-ndc})_2(dabco)$ (DUT-8(Ni))

Herbert C. Hoffmann,[†] Bassem Assfour,[‡] Fanny Epperlein,[†] Nicole Klein,[§] Silvia Paasch,[†] Irena Senkovska,[§] Stefan Kaskel,[§] Gotthard Seifert,[‡] and Eike Brunner*[,†]

[†]Bioanalytische Chemie, [‡]Physikalische Chemie, and [§]Anorganische Chemie I, Technische Universität Dresden, Fachrichtung Chemie und Lebensmittelchemie, 01062 Dresden, Germany

Supporting Information

ABSTRACT: Recently, we have described the metal−organic framework $Ni_2(2,6\text{-ndc})_2(dabco)$, denoted as DUT-8(Ni)[1] (DUT = Dresden University of Technology, 2,6-ndc = 2,6-naphthalenedicarboxylate, dabco = 1,4-diazabicyclo[2.2.2]octane). Upon adsorption of molecules such as nitrogen and xenon, this material exhibits a pronounced gate-pressure effect which is accompanied by a large change of the specific volume. Here, we describe the use of high-pressure in situ ^{129}Xe NMR spectroscopy, i.e., the NMR spectroscopic measurements of xenon adsorption/desorption isotherms and isobars, to characterize this effect. It appears that the pore system of DUT-8(Ni) takes up xenon until a liquid-like state is reached. Deeper insight into the interactions between the host DUT-8(Ni) and the guest atom xenon is gained from ab initio molecular dynamics (MD) simulations. van der Waals interactions are included for the first time in these calculations on a metal−organic framework compound. MD simulations allow the identification of preferred adsorption sites for xenon as well as insight into the breathing effect at a molecular scale. Grand canonical Monte Carlo (GCMC) simulations have been performed in order to simulate adsorption isotherms. Furthermore, the favorable influence of a sample pretreatment using solvent exchange and drying with supercritical CO_2 as well as the influence of repeated pore opening/closure processes, i.e., the "aging behavior" of the compound, can be visualized by ^{129}Xe NMR spectroscopy.

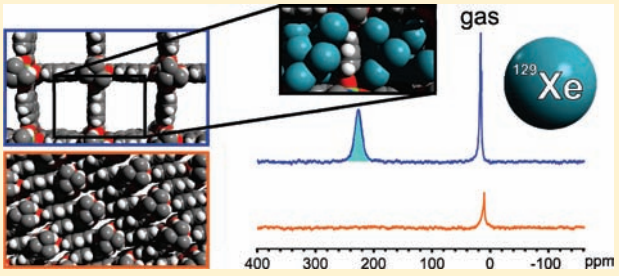

INTRODUCTION

Metal−organic frameworks (MOFs)[2−4] represent a class of hybrid materials built from organic and inorganic building blocks.[5] The interactions between organic and inorganic constituents are relatively strong,[6] resulting in two- or three-dimensional network structures.[5] In most cases, these networks exhibit micro- or mesopores and a huge internal surface area. Both hydrophilic and hydrophobic regions are often present in the MOF structure.[7] Usually, the density of MOFs is lower than 1 g/cm^3. In comparison with covalent or ionic bonds, however, the interactions between organic and inorganic compounds present in the MOF lattices are relatively weak: i.e., on the order of 100 kJ/mol. It is, therefore, not surprising that MOFs can be very flexible in comparison with typical porous solids such as zeolites and activated carbons under certain circumstances.[8] The flexibility of MOF frameworks, accompanied by crystalline structures, gives rise to the collective or cooperative effect,[8] which is capable of causing huge structural changes,[9] a strategy that is analogous to protein folding in nature. These pronounced reversible structural changes are denoted as breathing effects.[10] If the structural changes are large enough, they finally result in the so-called gate-pressure effect.[11] The previously "closed" structure opens at a certain threshold pressure: i.e., pressure-induced adsorption of special molecules takes place. $Ni_2(2,6\text{-ndc})_2(dabco)$ (DUT-8(Ni)) possesses a pillar-layered structure (see Figure 1, top) and exhibits a very pronounced gate-pressure effect during adsorption of molecules such as nitrogen, carbon dioxide, and xenon as well as for *n*-butane under given conditions.[1]

Applications of MOFs are suggested in catalysis,[12−15] in gas storage (for example, of hydrogen[14,16] or methane[17,18]), for gas and solvent purification,[19−21] and as nano reactors.[3] Furthermore, they may be useful as highly selective molecular sieves, as sensors,[22−27] in microelectronics,[28] as well as for optical purposes. The latter applications are due to the unusual magnetic, electronic, and optical effects found in several MOFs such as magnetic coupling of paramagnetic metal centers,[29] magnetic spin frustration,[30] fluorescence,[31] nonlinear optical properties,[32] flexibility,[33] and electronic or ionic conductivity/semiconductivity.[7]

Magnetic resonance spectroscopy is a well-established tool for the characterization of porous materials as well as their interactions with adsorbed species (host−guest interactions). For example, ^{1}H and ^{13}C magic-angle-spinning nuclear magnetic resonance (MAS NMR),[34−36] ^{71}Ga MAS NMR,[37] and diffusion

Received: March 3, 2011
Published: May 04, 2011

 © 2011 American Chemical Society

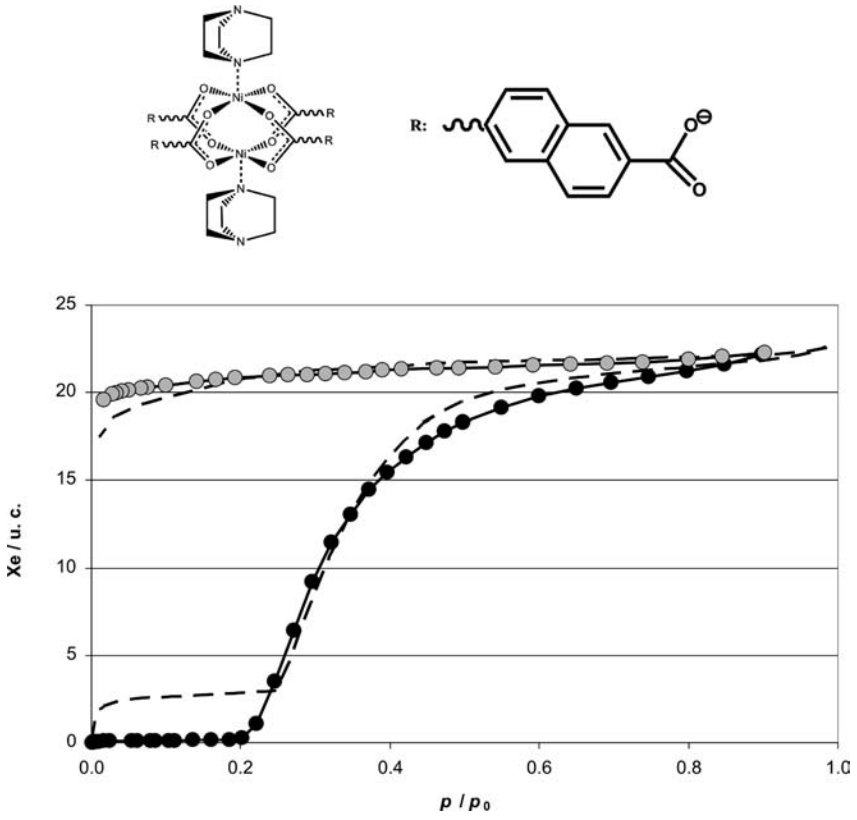

Figure 1. (Top) Paddle-wheel unit of DUT-8(Ni), built from two nickel atoms coordinated by four 2,6-ndc linkers and two dabco pillar ligands. (Bottom) Xenon adsorption/desorption isotherm of DUT-8(Ni) after sample pretreatment with supercritical CO_2 measured at 165 K: (filled circles) adsorption isotherm; (open circles) desorption isotherm; (dashed lines) adsorption/desorption isotherm of a sample without supercritical CO_2 drying.[1] The xenon loading (Xe/unit cell) is referred to the unit cell of the open DUT-8(Ni) containing 132 atoms.[1]

measurements by pulsed field gradient (PFG) NMR[38] as well as electron paramagnetic resonance (EPR) spectroscopy[39] were previously used in order to study MOFs.

During the past decades, ^{129}Xe NMR spectroscopy has found numerous applications for the characterization of various types of porous materials.[40−53] It offers different parameters encoding information about the surface and pore systems under study. Such parameters are the chemical shift, the line width, the chemical shift anisotropy, and the longitudinal relaxation time T_1. The first application of ^{129}Xe NMR spectroscopy to MOFs was reported in 2006.[54] Subsequently, other authors made use of the favorable properties of ^{129}Xe NMR in order to study MOFs using either thermally polarized[55] or hyperpolarized[36,56] xenon. Recently, the xenon-induced structural changes in MIL-53(Al) were studied by xenon adsorption[57] using thermally polarized as well as hyperpolarized ^{129}Xe.[58] It appears that the pore system of MIL-53(Al) is contracted during xenon adsorption for pressures of about 1 bar at 273 K.[57] The first high-pressure ^{129}Xe NMR studies of activated DUT-8(Ni)—which has a yellow color as well as narrow pores—showed that the pore system opens and the color changes to green if a sufficiently high xenon pressure—the temperature-dependent gate-opening pressure—is applied.[1] Similar color and magnetization changes were reported for $[(C_5H_5)Ni\{P(S)R_2\}_2Ni(C_5H_5)]$[59] as well as for some MOF structures.[60] This behavior was attributed to the so-called spin crossover (SCO) effect.[59] The electronic properties of DUT-8(Ni) will, therefore, be the subject of further investigation. Beyond the gate-opening pressure, significant adsorption of xenon is observed. The problem with these preliminary studies was, however, that the sample had to be xenon-loaded outside the NMR magnet. This means that variation of the pressure during the measurement and pressure control during temperature variations inside the magnet were impossible.

Therefore, we have developed an apparatus allowing in situ xenon pressure regulation: i.e., inside the magnet (see Figure 2). This enables the study of xenon adsorption/desorption processes isothermally or isobarically by ^{129}Xe NMR spectroscopy. Using this novel apparatus, we have studied the MOF compound DUT-8(Ni) by the combined use of high-pressure in situ ^{129}Xe NMR spectroscopy and computer simulations. The properties of MOFs critically depend on the synthesis conditions[6,35] and further sample treatment.[61] In particular, complete solvent removal is often difficult to achieve, which influences the adsorption properties of the MOF. Therefore, an improved solvent extraction method based on supercritical drying as introduced by Hupp et al.[62] has been applied to DUT-8(Ni) within the present work.

Computer simulations were performed in order to obtain a better understanding of the interactions between xenon and the DUT-8(Ni) framework as well as the dynamics at an atomic/molecular scale. Grand canonical Monte Carlo (GCMC) simulations are used to predict xenon adsorption isotherms. Additionally, the preferred adsorption sites of xenon have been investigated using the molecular dynamics (MD) technique. We were also able to observe huge breathing effects leading to a "closed" structure of DUT-8(Ni) through MD simulations. Previously, density functional theory (DFT) and MD studies

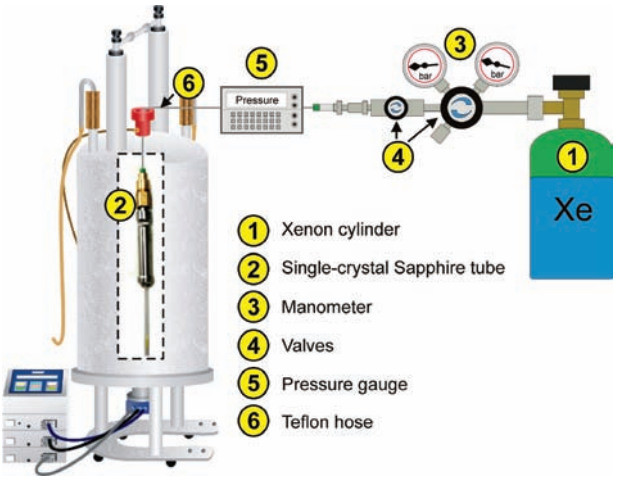

Figure 2. Scheme illustrating the homemade apparatus for high-pressure in situ ^{129}Xe NMR experiments at variable thermodynamic parameters.

related to the breathing of MIL-53(Cr)[63] were reported. However, ab initio MD simulations on MOFs, including van der Waals interactions, have not been reported before. As is shown in the present work, the inclusion of van der Waals interactions in the simulations is essential to get reliable results for the opening/closing behavior of DUT-8(Ni).

EXPERIMENTAL METHODS

DUT-8(Ni) was synthesized as described previously.[1] Sample activation was carried out by solvent exchange with subsequent supercritical CO_2 drying. The as-synthesized solid was washed twice with *N,N*-dimethylformamide (DMF) and immersed in acetone for 3 days to exchange the guest DMF/MeOH molecules with a solvent miscible with liquid CO_2. During this procedure, the acetone was replaced with fresh acetone three times. The samples were placed in a 13200J AB Jumbo Critical Point Dryer (SPI Supplies). The included acetone was exchanged with liquid carbon dioxide (purity 99.995%) at ~15−20 °C for about 20 h. The supercritical CO_2 was released at around 120 bar beyond the critical point, and the dryer was transferred into a glovebox. All samples were handled under inert gas (argon) atmosphere in a glovebox.

For xenon adsorption/desorption measurements, a Quantachrome Autosorb1C apparatus was extended by a cryostat from Oxford Instruments to perform the measurements up to 1 bar at 165 K.

^{129}Xe NMR experiments were performed on an Avance 300 spectrometer (Bruker, Karlsruhe, Germany) at a resonance frequency of 83.02 MHz using a 10 mm HR probe (6 μs pulse length). ^{129}Xe NMR spectroscopic studies were carried out using a new, homemade apparatus (see Figure 2) allowing sample pressurization directly inside the NMR magnet. The apparatus uses a high-pressure single-crystal sapphire tube equipped with a home-designed gas- and vacuumtight titanium valve similar to that described previously.[64] The apparatus can be connected to either a vacuum pump or an external gas reservoir. Chemical shifts were referenced by measuring the signal of xenon gas inside the tube at various pressures at room temperature and extrapolation of the chemical shift to zero pressure. The activated MOF sample is placed into the sapphire tube under an argon atmosphere. Afterward, the sample was evacuated under high vacuum at about 10^{-5} mbar. The sample tube was then transferred into the NMR spectrometer and connected to an outside xenon reservoir equipped with a pressure gauge using a Teflon hose. This allowed the sample to be pressurized in situ within the magnet. Using this equipment, we were able to measure ^{129}Xe NMR spectra under controlled

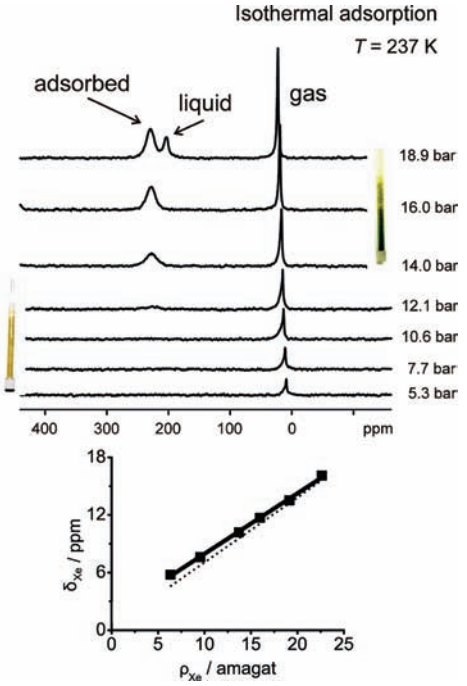

Figure 3. (Top) ^{129}Xe NMR spectra obtained for isothermal xenon adsorption (237 K) measured at various pressures on activated, evacuated supercritical CO_2 dried DUT-8(Ni) with initially "closed" pore system (yellow sample, see photograph on the left). The pore system opens at a gate pressure of ca. 12 bar, accompanied by a color change to green (see photograph on the right). Note that the top spectrum is not fully equilibrated, in contrast to the other spectra shown here. After equilibration, the signal due to liquid xenon is much stronger. (Bottom) Concentration dependence of the chemical shift of the gas-phase signal (solid squares and line) as well as chemical shift expected for pure xenon gas (dotted line).[79] Note that the xenon concentration ρ_{Xe} depends nonlinearly on the xenon pressure under the present conditions. One amagat corresponds to the density of xenon at a pressure of 1 atm and a temperature of 273 K.

temperature and at the desired pressure. The pressure was calibrated using the pressure sensor Heise ST-2H with a HQSC-2 Module. The uncertainty of the pressure inside the tube amounts to ±0.2 bar. The samples were allowed to equilibrate for at least 15 min after pressure changes and at least 30 min after temperature changes. ^{129}Xe NMR signals were monitored during this equilibration time in order to make sure that the signal remains constant after the equilibration period.

The temperature of the sample was calibrated as described in the literature by using the ^{1}H chemical shifts of methanol.[65−67] Since it is known that this method may exhibit systematic errors of a few degrees,[68,69] the temperature was calibrated by an independent second method. The condensation pressure of xenon was measured at the given temperature: i.e., the pressure where liquefaction starts inside the tube (see the Supporting Information, Figure S1). The corresponding temperature was then determined from the phase diagram of xenon found in the literature.[70] The temperature inside the tube was determined by averaging these two independent measurements (for the adsorption/desorption data shown in Figures 3 and 4, the temperature amounts to 237 ± 3 K).

COMPUTATIONAL METHODOLOGY

GCMC Simulations. GCMC simulations were performed to calculate the adsorption isotherms.[71,72] To evaluate the force field,

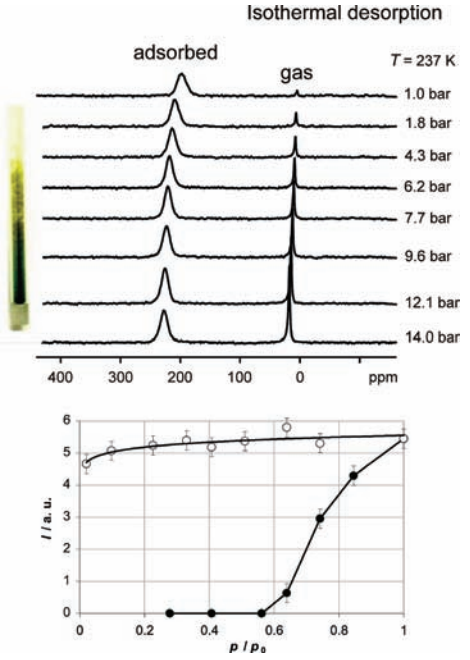

Figure 4. (Top) ^{129}Xe NMR spectra for isothermal desorption (237 K) of xenon measured at various pressures on a supercritical CO_2 dried DUT-8(Ni) sample following the adsorption process shown in Figure 3. The pore system remains open down to a pressure of 1 bar, as indicated by the constant green color of the sample (see photograph on the left). (Bottom) ^{129}Xe NMR derived adsorption/desorption isotherm for DUT-8(Ni) at 237 K: (filled circles) adsorption isotherm; (open circles) desorption isotherm. *I* denotes the intensity of the signal due to adsorbed xenon.

GCMC simulations were applied to predict xenon adsorption at the open DUT-8(Ni) structure up to 1 bar of xenon pressure at 165 K. These data could be compared with the experimental adsorption/desorption isotherms measured under the same conditions. The adsorption behavior of the simulated "closed" structure was calculated to prove its inaccessibility for xenon. For these GCMC simulations, we have used the structure predicted by MD simulations for the empty "closed" DUT-8(Ni) (see below).

DUT-8(Ni) was treated as a rigid lattice within the GCMC simulations. The atom positions for the open state were obtained by optimizing the experimentally determined crystal structure within a DFT approach (see below). Supercells were used as the GCMC simulation box. The supercells consisted of $2 \times 2 \times 4$ unit cells and contained more than 1000 atoms. For each point of the isotherm, the simulations were equilibrated for 20 000 000 steps. A further 20 000 000 steps were used for data sampling in order to ensure the convergence of the simulations. The nonbonding interactions between the framework of the MOF structure and xenon are described via a pairwise additive potential. The corresponding site−site interactions are described by a Lennard−Jones type potential. The standard universal force field (UFF)[73] was chosen to describe the xenon−framework interactions, whereas the xenon−xenon interaction parameters were taken from the literature.[74] Lorentz−Berthelot mixing rules were employed to calculate Xe-MOF Lennard−Jones potential parameters.

MD Simulations. Molecular dynamics and structural relaxation calculations were performed using DFT as implemented in the SIESTA simulation package.[75,76] The SIESTA code uses pseudopotentials, localized numerical basis sets, and periodic boundary conditions.

It is well-known that generalized gradient approximation (GGA) and local density approximation (LDA) fail to correctly account for van der Waals (vdW) interactions. Therefore, we have used a method described by Dion et al. to include van der Waals forces.[77] This method was successfully used, for example, to simulate the dynamic properties as well as to calculate the binding energy of H_2 adsorbed in MOF-74.[78]

The unit cell of the open structure of DUT-8(Ni), which contains 132 atoms, is known from single-crystal X-ray experiments.[1] It is, therefore, used as the starting point for all calculations. This initial open structure was first relaxed by a conjugate gradient scheme, and the energy of the minimized configuration was calculated. It should be emphasized that no experimental information about the "closed" structure is available yet. We, therefore, aimed to predict the "closed" structure by MD simulations using a DFT method which accounts for van der Waals interactions (DFT-vdW) as explained below. These simulations also monitored breathing effects during loading of the DUT-8(Ni) structure with xenon.

It is known from MIL-53(Al) that the Xe−MOF interactions can be sufficiently strong to contract the initially open pore system significantly.[57,58] In order to understand the influence of adsorbed xenon upon the structure of DUT-8(Ni), the following approach was chosen: two different amounts of xenon atoms were put into the optimized open DUT-8(Ni) unit cell. The final configurations obtained from the GCMC simulations described above were chosen as initial guesses for subsequent MD simulations. The MD simulations were performed within an NPT ensemble (constant number of particles, pressure, and temperature) using the Nosé−Parrinello−Rahman thermostat as implemented in SIESTA. Initially, the structure was equilibrated over 1 ps at 230 K. We have performed a subsequent MD simulation over 4 ps at 230 K with a step size of 1.0 fs. This procedure allows the investigation of the structural breathing in a rather unbiased manner. The results from the MD simulation for a loading of 10 xenon atoms per unit cell (Xe/uc)—where partial structure closing was found—were then used to predict the empty "closed" structure of DUT-8(Ni). The structure obtained from the MD simulation was used as an initial guess of the "closed" structure. The xenon atoms were removed, and full structural relaxation was performed. This procedure resulted in the "closed" structure without adsorbed xenon (empty "closed" structure).

The energetically preferred adsorption sites of xenon in DUT-8(Ni) were also determined. First, we optimized the cell of the empty but hypothetically open DUT-8(Ni) structure. Afterward, 19 Xe/uc—corresponding to the adsorption capacity predicted by GCMC simulations for 1 bar and 230 K—were put into the optimized structure followed by full structural relaxation. The xenon binding energy E_B at each of the revealed adsorption sites was calculated from the difference between the energy of the relaxed structures with adsorbed xenon, E(MOF + Xe), and the energy of the same structure after xenon removal, E(MOF). A correction accounting for the energy of free xenon in the same but empty unit cell E(Xe) was furthermore applied:

$$E_B = E(\mathrm{MOF} + \mathrm{Xe}) - E(\mathrm{MOF}) - E(\mathrm{Xe}) \quad (1)$$

A 16k-point mesh was found to be sufficient for the total energy to converge within 0.1 meV/atom.

RESULTS AND DISCUSSION

Adsorption Isotherms. Figure 1 (bottom) shows the xenon adsorption/desorption isotherm of supercritical CO_2 dried DUT-8(Ni) measured up to 1 bar at 165 K. For comparison, the xenon adsorption data published previously[1] for DUT-8(Ni) without the postsynthetic supercritical CO_2 drying is also shown (dashed line). The adsorption isotherms nicely agree, apart from one major difference. No measurable amount of xenon is adsorbed in the supercritical CO_2 dried sample below the gate-opening pressure. In contrast, the non-CO_2-dried sample was capable of adsorbing a certain amount of xenon—ca. 2.5 Xe/uc—even below the gate-opening pressure.[1] For the supercritical

dx.doi.org/10.1021/ja201951t | J. Am. Chem. Soc. 2011, 133, 8681–8690

CO_2 dried DUT-8(Ni) samples, however, the pore system is entirely "closed" for xenon below the gate-opening pressure. Beyond the gate-opening pressure of $p/p_0 \approx 0.2$ at 165 K, both samples—with and without supercritical CO_2 drying—rapidly take up a large amount of xenon until the saturation value of ca. 22 Xe/uc is reached. Pressure release down to relative pressures of 0.017 only results in minor changes of the amount of xenon adsorbed within the pore system (Xe@DUT-8(Ni)): i.e., a pronounced hysteresis.

High-Pressure in Situ ^{129}Xe NMR Spectroscopy. Figure 3 displays the ^{129}Xe NMR spectra of supercritical CO_2 dried DUT-8(Ni) measured at 237 K. Below a pressure of ca. 12 bar, the spectrum only exhibits a single signal. Its concentration-dependent, i.e., pressure-dependent, chemical shift falls within the range of 5−20 ppm (Figure 3, bottom). This signal is attributed to gaseous xenon. Its chemical shift (filled squares, solid line) slightly exceeds the chemical shift of pure xenon gas (dotted line) reported in the literature.[79] It should be noted that we have also measured the chemical shift of gaseous xenon in our apparatus without any sample and observed an excellent agreement between our data and the values reported by Jameson et al.[79] (see the Supporting Information, Figure S1). The increased chemical shift indicates that the xenon atoms giving rise to this signal are occupying the free space between the MOF particles in the powder sample and the macropores of the MOF particles. Due to their interactions with the external surface of the particles, the chemical shift is increased with respect to free gas atoms[79] (see also the Supporting Information, Figure S2). It is well known that the chemical shift of xenon (δ) can be written as the sum of several contributions:[40,44−47]

$$\delta = \delta_0 + \delta_S + \delta_{Xe-Xe}\rho_{Xe} + \delta_E + \delta_M \qquad (2)$$

The chemical shift at zero pressure, δ_0, is set to zero by calibration. δ_S arises from xenon−surface interactions. $\delta_{Xe-Xe}\rho_{Xe}$ is due to xenon−xenon interactions; it, therefore, depends on the density of xenon. δ_E and δ_M are the contributions from interactions with electrostatic fields and paramagnetic sites, respectively. The aforementioned increase of the chemical shift in comparison with that for the gas phase is explained by the interactions of gaseous xenon with the external surface of the microcrystalline DUT-8(Ni) particles. It should be noted that this effect consequently depends on the packing density of the particles (see also the Supporting Information, Figure S2, middle).

The sample remains yellow below the gate-opening pressure (see insert), indicating that the pore system is "closed". Furthermore, an increasingly strong signal at 227 ppm is observed beyond 12 bar, the gate-opening pressure at 237 K. This signal slightly shifts to 229 ppm at increasing pressure. The appearance of this signal is accompanied by a characteristic color change of the sample from yellow to green (see insert). This color change is indicative of pore opening.[1] The observed chemical shift of 227 ppm is close to the value characteristic for liquid xenon. However, it can be excluded that the latter signal is simply due to liquid xenon outside the MOF particles for several reasons.

(i) The phase diagram of xenon predicts the onset of liquefaction at 237 K beyond 17 bar.[70] Indeed, the characteristic signal due to liquid xenon outside the MOF particles occurs in the spectrum measured at 18.9 bar (see Figure 3) and higher pressures at a chemical shift of 203 ppm. Note that the spectrum shown in Figure 3 was not allowed to fully equilibrate, in contrast to the other spectra shown here. After full equilibration, the signal at 203 ppm due to liquid xenon becomes very intense and the gas-phase signal entirely disappears (see the Supporting Information, Figures S3 and S4).

(ii) Furthermore, the signal due to liquid xenon at 203 ppm disappears if the applied xenon pressure is lowered afterward. In contrast, the intensity of the signal at 229 ppm (at 18.9 bar) remains almost constant if the pressure drops ("hysteresis"), as demonstrated in Figure 4.

(iii) The aforementioned characteristic color change from yellow to green clearly indicates the pore-opening process beyond 12 bar at 237 K. The signal in the range of 225−230 ppm is, therefore, definitely due to Xe@DUT-8(Ni).

It is remarkable that the line width of this signal amounts to only 1400 Hz. This is much less than the line width of ca. 4000 Hz previously observed for xenon adsorbed in DUT-8(Ni) without the supercritical CO_2 drying.[1] It is, furthermore, remarkable that the supercritical CO_2 dried sample does not exhibit a signal due to Xe@DUT-8(Ni) below the gate-opening pressure, in agreement with the adsorption/desorption isotherm shown in Figure 1. In contrast, the sample without supercritical CO_2 drying exhibits a relatively weak and broad (ca. 6000 Hz) ^{129}Xe NMR signal due to Xe@DUT-8(Ni) even below the gate-opening pressure, as reported previously.[1] The aforementioned broad signal exhibited an anisotropy as well as chemical shift values higher than the narrow signal of xenon on supercritical CO_2 dried DUT-8(Ni). This shows that DUT-8(Ni) without supercritical CO_2 drying exhibits a narrow pore state for xenon, as reported for MIL-53(Al).[58] The total absence of a signal due to adsorbed xenon for the supercritical CO_2 dried samples shows that the sample pretreatment with supercritical CO_2 results in an improved pore opening/closing behavior of the sample. In agreement with the aforementioned adsorption measurements, ^{129}Xe NMR also shows that supercritical CO_2 dried DUT-8(Ni) is entirely "closed" for xenon below the gate-opening pressure. The observation of a much narrower ^{129}Xe NMR signal for the open state after supercritical CO_2 drying indicates a more homogeneous environment for Xe@DUT-8(Ni). This effect may be related to improved solvent removal or/and "healing" of crystal lattice defects caused by the treatment in supercritical CO_2.

The chemical shift in the range of 225−230 ppm for the signal due to Xe@DUT-8(Ni) points toward a liquid-like state and density of the adsorbed xenon. In order to verify this idea, we have estimated the density of xenon inside the fully occupied pore system. The pore volume of 0.99 cm^3/g estimated by computer simulations using the nonadsorbing noble gas helium as a probe agrees remarkably well with the experimentally determined total pore volume of 1.05 cm^3/g (N_2 physisorption, $T = 77$ K, $p/p_0 = 0.95$). Xenon concentrations of 25 and 22 Xe/uc were derived from the GCMC simulation and the xenon adsorption isotherm ($T = 165$ K, Figure 1), respectively. These values correspond to xenon densities inside the pore system of 2.52 and 2.34 g/cm^3, respectively. The density of liquid xenon amounts to 2.94 g/cm^3 at 1.01 bar and 165 K. This means that the xenon densities observed in the pore system of DUT-8(Ni) are indeed close to the liquid state. Furthermore, the signal caused by adsorbed xenon inside the pore system (Xe@DUT-8(Ni)) does not change if liquid xenon is formed around the MOF particles (see the Supporting Information, Figures S3 and S4). Were the density inside the pore system of gas-surrounded particles significantly lower than that of liquid xenon, the

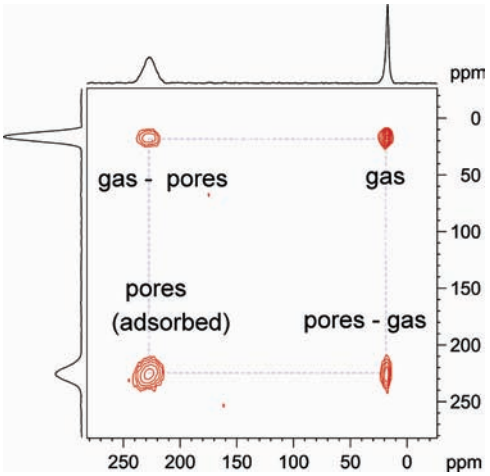

Figure 5. 2D ^{129}Xe EXSY NMR spectrum measured at 237 K and 15 bar with a mixing time of 25 ms. The presence of cross-peaks indicates exchange between Xe@DUT-8(Ni) and the gas phase.

formation of a liquid phase around the particles should be accompanied by an increasing xenon density also inside the pores. This is, however, not observed. It is, therefore, concluded that xenon adsorption in the pore system of DUT-8(Ni) results in the formation of a liquid-like phase.

It should, furthermore, be mentioned that DUT-8(Ni) is a paramagnetic compound. For channels decorated with paramagnetic centers, the ^{129}Xe NMR signals are expected to exhibit a characteristic line broadening and shift.[80] In the case of the paramagnetic DUT-8(Ni), a rigorous theoretical treatment has not yet been performed. However, its magnetization in the open and "closed" state is known[1] and allows the estimation of an expected average paramagnetic shift contribution of about 21 ppm for the open state. This estimated paramagnetic shift is close to the observed chemical shift difference of 26 ppm between the liquidlike Xe@DUT-8(Ni) (229 ppm) and liquid xenon outside the pores (203 ppm). The narrow line width of ca. 1400 Hz for the signal of Xe@DUT-8(Ni) shows that the paramagnetic nickel sites do not give rise to strong line broadening. This behavior can be explained by the relatively high mobility of xenon, which results in motional averaging of possible field inhomogeneities inside the pore system and/or a relatively homogeneous paramagnetic field contribution inside the material. Therefore, the paramagnetic contribution should exhibit a $1/T$ dependence. A corresponding behavior which can approximately be described by a $1/T$ dependence is indeed observed (see the Supporting Information, Figure S5). However, other terms in eq 2 will also contribute to this temperature dependence.

Figure 5 exhibits the 2D ^{129}Xe EXSY spectrum (EXSY = exchange spectroscopy). This experiment shows that the xenon atoms inside the pore system of DUT-8(Ni) exchange rapidly with the surrounding gas phase at a time scale of tens of milliseconds, as indicated by characteristic cross-peaks at the mixing time of 25 ms. This magnitude of exchange time agrees well with values observed in other MOFs.[36]

The gate-opening temperature at which the pore system opens for xenon is pressure-dependent.[1] It amounts to 237 K at ca. 12 bar for the activated, evacuated, and xenon-loaded sample, as shown in Figure 3. However, this temperature systematically increases if the pore opening/closing process is repeated. In order to quantify this change, we have measured adsorption isobars: i.e.,

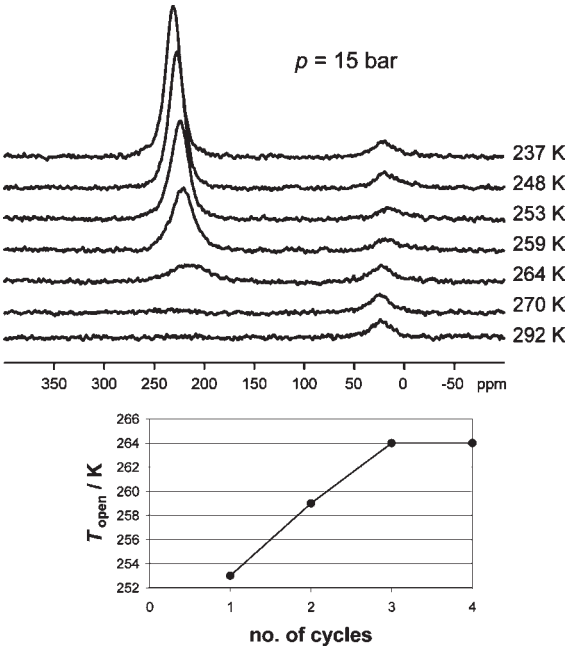

Figure 6. (Top) Variable-temperature ^{129}Xe NMR spectra of xenon adsorbed at constant pressures (15 bar) on a supercritical CO_2 dried DUT-8(Ni) sample following three subsequent pore opening/closing cycles. Note that the pore-opening temperature has now shifted up to ca. 264 K. (Bottom) Pore-opening temperature at 15 bar of xenon pressure as a function of the number of repeated opening/closing cycles. We define the gate-opening temperature as the temperature where the ^{129}Xe NMR signal of xenon inside the pore system appears in the spectrum.

we have cooled a sample several times at a constant external pressure of 15 bar until the pore system opened, as indicated by the characteristic signal at 225−230 ppm by ^{129}Xe NMR spectroscopy as well as the characteristic green color of the sample. Afterward, the sample was heated to room temperature and evacuated, resulting in the complete closure of the pore system, as indicated by the disappearance of the signal at 225−230 ppm as well as the characteristic yellow color of the sample. After three pore opening/closing cycles, the gate-opening temperature reached a value of ca. 264 K at 15 bar (see Figure 6). It should, furthermore, be noted that the chemical shift of the signal due to Xe@DUT-8(Ni) slightly changed to a final value of 231 ppm and the line width increased to about 1500 Hz. Obviously, the repeated pore opening/closing cycles result in minor structural changes/rearrangements within the crystal lattice, giving rise to the observed change of the gate-opening temperature as well as the slight changes in chemical shift and line width.

Computer Simulations. The structure is not flexible during GCMC simulations: i.e., it is fixed in its open state. Therefore, the simulated adsorption data must be compared with the experimentally determined xenon desorption isotherm. Figure 7 shows the calculated amount of xenon adsorbed in the open structure at 165 K (squares) in comparison with the experimental xenon desorption isotherm (circles). The GCMC results are in good agreement with the experimental xenon desorption measurements. The calculations predict a xenon adsorption capacity slightly higher than that experimentally determined. Similar deviations are well-known from the literature.[72,81,82] They can be attributed to experimental imperfections such as the presence of residual solvent molecules or defects in the crystal structure. In contrast,

dx.doi.org/10.1021/ja201951t |J. Am. Chem. Soc. 2011, 133, 8681–8690

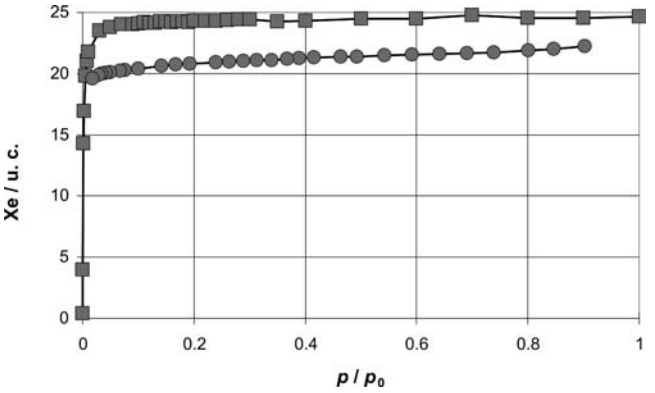

Figure 7. Comparison of the experimental xenon desorption isotherm as shown in Figure 1 (circles) with the GCMC-derived xenon adsorption capacity calculated for the open structure (squares) at 165 K.

the simulations are performed on idealized structures without solvent molecules or distortions. Since the GCMC calculations do not account for thermal motions, the accessible pore volume and thus the xenon loading may be overestimated further.

The experimentally observed xenon adsorption and NMR measurements indicate a "closed", i.e., xenon-inaccessible, structure below the gate-opening pressure. Geometry optimization of the experimentally determined crystal structure did not result in any significant changes: i.e., the result (structure 1 in Figure 8) corresponds to the experimentally determined structure. The specific volume of the relaxed structure of 3230 Å^3/uc agrees well with the specific volume of 3190 Å^3/uc of the structure obtained from X-ray diffraction at room temperature containing DMF/MeOH inside the pores (see the CIF files, available in the Supporting Information).

However, the open structure is experimentally observed only for the as-synthesized solvent-filled material or for the activated material after subsequent adsorption of molecules such as xenon beyond the gate-opening pressure. Otherwise the real empty DUT-8(Ni) exhibits a "closed" structure in the temperature range studied yet (77 K to ca. 300 K). Therefore, the open structure was computationally subjected to an external xenon pressure of 1 bar at 230 K in the corresponding GCMC simulations. It is important to note that the NMR experiments (see Figure 4) clearly show that the structure remains open at 1 bar of external xenon pressure, even at 237 K. The GCMC simulations predict a xenon adsorption capacity of 19 Xe/uc for the open structure at 1 bar and 230 K. This is close to the experimental value of 22 Xe/uc derived as the maximum adsorption capacity at 165 K (see the adsorption isotherm in Figure 1). With this amount of xenon added, the DUT-8(Ni) structure remains open after geometry optimization (see structure 4 in Figure 8), in agreement with the experimental observations described above.

The experimental data furthermore show that the structure closes if the adsorbed molecules are removed: i.e., for zero loading. In order to simulate this structure-closing process, the amount of xenon put into the open structure was reduced. Using a xenon loading of only 10 Xe/uc, MD simulations show a significant contraction of the crystal lattice. The unit cell volume decreases from 3230 Å^3 to a volume of 1950 Å^3: i.e., it shrinks by about 40% (structure 2 in Figure 8, see also the CIF files in the Supporting Information). This behavior is explained by relatively

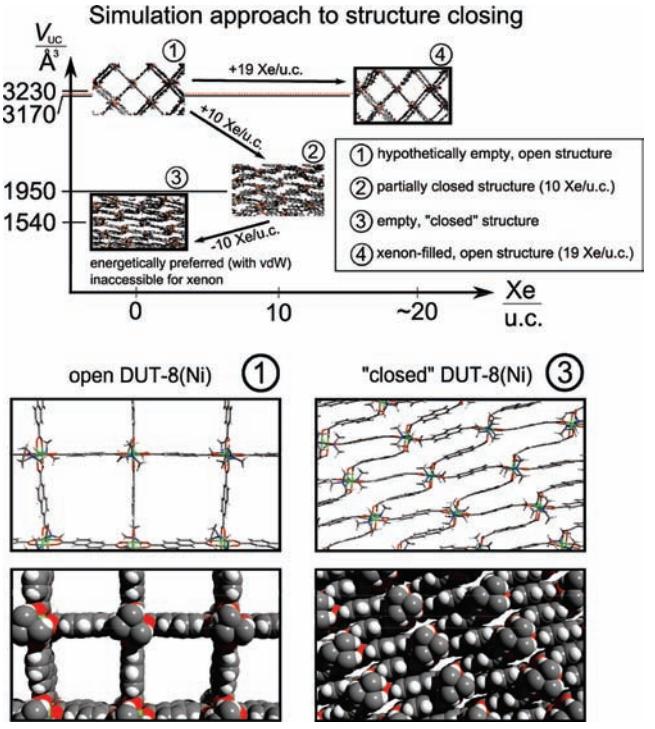

Figure 8. (Top) Scheme of the computational approach for observing the closure of the DUT-8(Ni) structure. The starting point is the experimentally determined open structure[1] after relaxation (structure 1). If structure 1 is loaded with an amount of xenon corresponding to the predicted adsorption capacity (19 Xe/uc), it remains open and the volume of the unit cell only drops slightly (structure 4). If 10 Xe/uc is put into structure 1, MD simulations result in a partially closed structure (structure 2). Subsequently, xenon is totally removed from this hypothetical transition structure. MD simulations then result in structure 3. It is important to note that the "closed" structure 3 is only stable if DFT-vdW is applied. Without the inclusion of van der Waals forces, structure 1 is energetically favored instead of structure 3. The unit cell volumes for structures 1 and 3 are shown for the geometrically optimized unit cells. The red dashed line denotes the unit cell volume of 3190 Å^3/uc for the experimentally determined open structure. (Bottom) Comparison of experimentally determined open and predicted "closed" structures of DUT-8(Ni) in stick design (top) and van der Waals illustration (bottom), respectively. Nickel, hydrogen, carbon, nitrogen, and oxygen atoms are shown in green, white, gray, blue, and red, respectively. Xenon atoms are omitted for clarity.

strong van der Waals interactions between xenon and the DUT-8(Ni) framework and illustrates the pronounced structural flexibility of DUT-8(Ni). Note that the calculated partially closed structure (10 Xe/uc) should be considered as a hypothetical intermediate state, because structure closing is a rather collective effect accompanied by rapid xenon desorption. In contrast, the xenon atoms put into the structure cannot leave the unit cell in our computer simulations. The calculated partially closed structure containing 10 Xe/uc (structure 2 in Figure 8) was then further relaxed after removing all xenon atoms from the unit cell. Total xenon removal resulted in a further unit cell contraction down to a final volume of 1540 Å^3 for the empty structure, corresponding to ca. 50% of the specific volume of the open structure. In agreement with our experimental observations, this calculated "closed" structure is found to be inaccessible for xenon (see structure 3 in Figure 8, bottom). DFT-vdW calculations indicate that the energy of the predicted empty "closed" structure

dx.doi.org/10.1021/ja201951t |J. Am. Chem. Soc. 2011, 133, 8681–8690

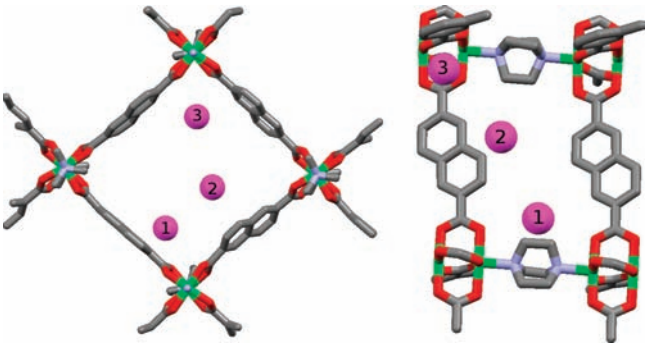

Figure 9. Preferred adsorption sites for xenon in the unit cell of DUT-8(Ni) as predicted by MD simulations: (1) close to the pillar ligand dabco; (2) near the 2,6-ndc linker; (3) close to the two nickel atoms at the paddle-wheel unit. The atoms are shown in the same colors as in Figure 8. Xenon atoms are shown in pink. Hydrogen atoms are omitted for clarity.

is 136 kJ/(mol uc) lower than that of the hypothetical empty open DUT-8(Ni) (structure 1 in Figure 8). This is in agreement with the experimental observation that DUT-8(Ni) prefers the "closed" state below the gate-opening pressure. It is important to note that the empty "closed" structure was only found to be stable in our DFT calculations if van der Waals interactions were explicitly included (DFT-vdW). This observation is in good agreement with a DFT study on MIL-53(Cr),[63] where no dispersion correction had been applied. No stable narrow pore state could be achieved in these calculations, although thermodynamic measurements and simulations including van der Waals interactions[83] indicate a narrow pore state for the MIL-53 family at 0 K.[57] In analogy, the empty "closed" structure of DUT-8(Ni) is also unstable if DFT is applied in LDA or GGA approximations. This means that the explicit inclusion of van der Waals interactions is crucial for the simulation of the structure closing process induced by xenon removal from DUT-8(Ni). The distance between the two 2,6-ndc linkers observed in the predicted "closed" structure amounts to ca. 330 pm. We, therefore, conclude that the "closed" structure is mainly stabilized by $\pi-\pi$ stacking of the 2,6-ndc linkers.

Our computer simulations also allow the calculation of adsorption energies. The highest values are predicted for three different sites, as shown in Figure 9. The first one is located close to the pillaring ligand dabco and exhibits an adsorption energy of 25 kJ/mol. The second one is close to the 2,6-ndc linker with an adsorption energy of 17 kJ/mol. The third preferred adsorption site is located near the two nickel atoms of the paddle-wheel unit. The predicted adsorption energy amounts to 7 kJ/mol. No direct interaction with the metal cluster was found to be energetically preferred. These preferred xenon adsorption sites predicted for DUT-8(Ni) are similar to those found for hydrogen in MIL-53(Cr).[84] Analogously, the strongest adsorption sites are located close to the organic linkers. The average adsorption energy calculated for a loading with 19 Xe/uc amounts to ~18 kJ/mol, in complete agreement with literature data reported for other metal–organic frameworks.[55−58]

A number of attempts to theoretically understand the pore opening/closing behavior of flexible porous materials have been previously described.[85−89] One model describes the breathing transitions between the narrow-pore and the large-pore states of MIL-53 and the observed hysteresis in terms of the stress exerted upon the framework by gas adsorption.[85,86,88] This model may also help in understanding the behavior of other MOFs exhibiting a gate-pressure effect[86] such as DUT-8(Ni). The experiments on DUT-8(Ni) described here start with the "closed", i.e., xenon-inaccessible, pore system. In contrast to MIL-53, no measurable xenon adsorption is observed at low xenon pressures for DUT-8(Ni) (see Figures 1 and 3). This means that the probability for xenon to enter the "closed" crystallites is practically zero. As a result, the exerted stress is mainly governed by the external pressure. We assume that xenon atoms start entering the pores at sufficiently high external gas pressure: i.e., the probability for xenon to overcome the gas–crystallite interface does then increase. The exact mechanism of this initial step toward pore opening is, however, not yet known. Furthermore, the real gas–crystallite interface—containing imperfections and macropores—is likely to be important for this initial step. This influence is, however, hardly detectable or accessible for calculations. The xenon atoms are then increasingly adsorbed in the initially closed framework, thus exerting stress on it. The state of the system will then be determined by Xe-MOF, MOF-MOF (linker–linker), and xenon–xenon interactions. As an increasing number of xenon atoms enters the pores, the internal stress caused by the xenon atoms becomes sufficiently large at a certain point and overrides the external stress and the attractive interactions within the MOF lattice: i.e., the structure opens. Therefore, the breathing process should also be discussed with respect to the calculated interaction energies. The calculated energy difference of 136 kJ/(mol uc) (see above) between the hypothetically open and the "closed" structure in the empty state must be overcome during the adsorption-induced pore-opening process. In the open state, one unit cell contains ca. 19 xenon atoms with a calculated average adsorption energy of 18 kJ/mol (see above). This would correspond to an overall xenon adsorption energy of ca. 340 kJ/(mol uc) for the xenon-filled open structure. The latter value clearly exceeds the calculated energy difference of 136 kJ/(mol uc) between the empty open and closed structures. It should be noted that repulsive xenon–xenon interactions may result in a lowering of the overall energy gain. Nevertheless, the reason for the opening process from an energetic point of view seems to be the stabilization of the open DUT-8(Ni) structure by attractive Xe–MOF interactions which overcompensate the $\pi-\pi$ interactions of the 2,6-ndc linkers in the closed structure.

■ CONCLUSIONS

The flexible and paramagnetic MOF DUT-8(Ni) was studied by the combined use of high-pressure in situ ^{129}Xe NMR spectroscopy and GCMC as well as MD simulations. The pore-opening process is accompanied by the observation of a narrow ^{129}Xe NMR signal at a chemical shift in the range of 225–230 ppm. These values even exceed the chemical shift of liquid xenon outside the crystallites (203 ppm). This behavior is accompanied by the observation of a very high xenon density inside the compound close to that of liquid xenon. This means that our observations indicate the stabilization of a liquidlike phase inside the pore system. 2D EXSY experiments reveal that the xenon atoms inside the pore system of DUT-8(Ni) exchange rapidly with the surrounding gas phase (interspace between particles = macropores). GCMC simulations agree well with experimental desorption measurements for the open DUT-8(Ni). Furthermore, a pronounced "breathing" is revealed by our

computer simulations if xenon is removed from the structure. This finally leads to an empty "closed" structure, as predicted by using MD simulations with DFT-vdW. To the best of our knowledge, this is the first time that DFT-vdW has been applied in MD simulations of a MOF compound. The use of a DFT method which accounts for van der Waals interactions turned out to be crucial, because the stability of the "closed" structure appears to be caused by van der Waals interactions between the 2,6-ndc linkers. These linkers exhibit $\pi-\pi$-stacking. The calculated structure does not exhibit pores large enough to allow the penetration of xenon into the "closed" metal−organic framework, in complete agreement with adsorption measurements and ^{129}Xe NMR spectroscopy. The favorable influence of a postsynthetic supercritical CO_2 drying on the adsorption properties is reflected by the NMR parameters. The preferred adsorption sites and interaction energies of xenon atoms in the open DUT-8(Ni) could also be determined by MD simulations using the DFT-vdW method.

■ ASSOCIATED CONTENT

Supporting Information. Figures S1−S5, giving ^{129}Xe NMR spectra, a scheme showing the influence of the NMR spectrometer, and the $1/T$ dependence of the Xe@DUT-8(Ni) signal, and CIF files giving crystallographic data for structures **1**−**4**. This material is available free of charge via the Internet at http://pubs.acs.org.

■ AUTHOR INFORMATION

Corresponding Author
*E-mail: eike.brunner@tu-dresden.de.

■ ACKNOWLEDGMENT

Financial support from the Deutsche Forschungsgemeinschaft (SPP 1362) is gratefully acknowledged. Thanks are further due to Dr. Stefano Leoni for helpful discussions, Ms. Annett Bachmann and Ms. Renate Schulze (Dresden) for carefully proofreading the manuscript, and the Zentrum für Informationsdienste und Hochleistungsrechnen (ZIH) for delivering the computational resources.

■ REFERENCES

(1) Klein, N.; Herzog, C.; Sabo, M.; Senkovska, I.; Getzschmann, J.; Paasch, S.; Lohe, M. R.; Brunner, E.; Kaskel, S. *Phys. Chem. Chem. Phys.* **2010**, *12*, 11778.
(2) Kitagawa, S.; Kitaura, R.; Noro, S.-i. *Angew. Chem., Int. Ed.* **2004**, *43*, 2334.
(3) Férey, G. *Stud. Surf. Sci. Catal.* **2007**, *170*, 66.
(4) Kaskel, S. *Handb. Porous Solids* **2002**, *2*, 1190.
(5) Férey, G. *Dalton Trans.* **2009**, *23*, 4400.
(6) Rowsell, J. L. C.; Yaghi, O. M. *Microporous Mesoporous Mater.* **2004**, *73*, 3.
(7) Férey, G. *Chem. Soc. Rev.* **2008**, *37*, 191.
(8) Férey, G.; Serre, C. *Chem. Soc. Rev.* **2009**, *38*, 1380.
(9) Serre, C.; Millange, F.; Thouvenot, C.; Noguès, M.; Marsolier, G.; Louër, D.; Férey, G. *J. Am. Chem. Soc.* **2002**, *124*, 13519.
(10) Loiseau, T.; Serre, C.; Huguenard, C.; Fink, G.; Taulelle, F.; Henry, M.; Bataille, T.; Férey, G. *Chem. Eur. J.* **2004**, *10*, 1373.
(11) Li, D.; Kaneko, K. *Chem. Phys. Lett.* **2001**, *335*, 50.
(12) Czaja, A. U.; Trukhan, N.; Müller, U. *Chem. Soc. Rev.* **2009**, *38*, 1284.
(13) Ma, L.; Abney, C.; Lin, W. *Chem. Soc. Rev.* **2009**, *38*, 1248.
(14) Proch, S.; Herrmannsdörfer, J.; Kempe, R.; Kern, C.; Jess, A.; Seyfarth, L.; Senker, J. *Chem. Eur. J.* **2008**, *14*, 8204.
(15) Henschel, A.; Gedrich, K.; Kraehnert, R.; Kaskel, S. *Chem. Commun.* **2008**, 4192.
(16) Salles, F.; Kolokolov, D. I.; Jobic, H.; Maurin, G.; Llewellyn, P. L.; Devic, T.; Serre, C.; Férey, G. *J. Phys. Chem. C* **2009**, *113*, 7802.
(17) Noguchi, H.; Kondoh, A.; Hattori, Y.; Kanoh, H.; Kajiro, H.; Kaneko, K. *J. Phys. Chem. B* **2005**, *109*, 13851.
(18) Wang, H.; Getzschmann, J.; Senkovska, I.; Kaskel, S. *Microporous Mesoporous Mater.* **2008**, *116*, 653.
(19) Hamon, L.; Serre, C.; Devic, T.; Loiseau, T.; Millange, F.; Férey, G.; Weireld, G. D. *J. Am. Chem. Soc.* **2009**, *131*, 8775.
(20) Greathouse, J. A.; Kinnibrugh, T. L.; Allendorf, M. D. *Ind. Eng. Chem. Res.* **2009**, *48*, 3425.
(21) Li, J.-R.; Kuppler, R. J.; Zhou, H.-C. *Chem. Soc. Rev.* **2009**, *38*, 1477.
(22) Reineke, T. M.; Eddaoudi, M.; Fehr, M.; Kelley, D.; Yaghi, O. M. *J. Am. Chem. Soc.* **1999**, *121*, 1651.
(23) Chandler, B. D.; Côté, A. P.; Cramb, D. T.; Hill, J. M.; Shimizu, G. K. H. *Chem. Commun.* **2002**, 1900.
(24) Halder, G. J.; Kepert, C. J.; Moubaraki, B.; Murray, K. S.; Cashion, J. D. *Science* **2002**, *298*, 1762.
(25) Maspoch, D.; Ruiz-Molina, D.; Wurst, K.; Domingo, N.; Cavallini, M.; Biscarini, F.; Tejada, J.; Rovira, C.; Veciana, J. *Nat. Mater.* **2003**, *2*, 190.
(26) Allendorf, M. D.; Houk, R. J. T.; Andruszkiewicz, L.; Talin, A. A.; Pikarsky, J.; Choudhury, A.; Gall, K. A.; Hesketh, P. J. *J. Am. Chem. Soc.* **2008**, *130*, 14404.
(27) Serre, C.; Mellot-Draznieks, C.; Surblé, S.; Audebrand, N.; Filinchuk, Y.; Férey, G. *Science* **2007**, *315*, 1828.
(28) Real, J. A.; Andrés, E.; Muñoz, M. C.; Julve, M.; Granier, T.; Bousseksou, A.; Varret, F. *Science* **1995**, *268*, 265.
(29) Maspoch, D.; Ruiz-Molina, D.; Veciana, J. *J. Mater. Chem.* **2004**, *14*, 2713.
(30) Srikanth, H.; Hajndl, R.; Moulton, B.; Zaworotko, M. J. *J. Appl. Phys.* **2003**, *93*, 7089.
(31) Gándara, F.; de Andrés, A.; Gómez-Lor, B.; Gutiérrez-Puebla, E.; Iglesias, M.; Monge, M. A.; Proserpio, D. M.; Snejko, N. *Cryst. Growth Des.* **2008**, *8*, 378.
(32) Evans, O. R.; Lin, W. *Acc. Chem. Res.* **2002**, *35*, 511.
(33) Kitagawa, S.; Uemura, K. *Chem. Soc. Rev.* **2005**, *34*, 109.
(34) Müller, M.; Lebedev, O. I.; Fischer, R. A. *J. Mater. Chem.* **2008**, *18*, 5274.
(35) Lee, E. Y.; Jang, S. Y.; Suh, M. P. *J. Am. Chem. Soc.* **2005**, *127*, 6374.
(36) Comotti, A.; Bracco, S.; Sozzani, P.; Horike, S.; Matsuda, R.; Chen, J.; Takata, M.; Kubota, Y.; Kitagawa, S. *J. Am. Chem. Soc.* **2008**, *130*, 13664.
(37) Volkringer, C.; Loiseau, T.; Férey, G.; Morais, C. M.; Taulelle, F.; Montouillout, V.; Massiot, D. *Microporous Mesoporous Mater.* **2007**, *105*, 111.
(38) Stallmach, F.; Gröger, S.; Künzel, V.; Kärger, J.; Yaghi, O. M.; Hesse, M.; Müller, U. *Angew. Chem.* **2006**, *118*, 2177.
(39) Jiang, Y.; Huang, J.; Kasumaj, B.; Jeschke, G.; Hunger, M.; Mallat, T.; Baiker, A. *J. Am. Chem. Soc.* **2009**, *131*, 2058.
(40) Ito, T.; Fraissard, J. *J. Chem. Phys.* **1982**, *76*, 5225.
(41) Raftery, D.; Long, H.; Meersmann, T.; Grandinetti, P. J.; Reven, L.; Pines, A. *Phys. Rev. Lett.* **1991**, *66*, 584.
(42) Springuel-Huet, M. A.; Fraissard, J. *Chem. Phys. Lett.* **1989**, *154*, 299.
(43) Demarquay, J.; Fraissard, J. *Chem. Phys. Lett.* **1987**, *136*, 314.
(44) Ripmeester, J. A.; Ratcliffe, C. I. *J. Phys. Chem.* **1990**, *94*, 7652.
(45) Barrie, P. J.; Klinowski, J. *Prog. Nucl. Magn. Res. Spectrosc.* **1992**, *24*, 91.
(46) Raftery, D.; Chmelka, B. *NMR Basic Princ. Prog.* **1994**, *30*, 111.
(47) Ratcliffe, C. I. *Annu. Rep. NMR Spectrosc.* **1998**, *36*, 123.
(48) Brunner, E. *Concepts Magn. Reson. A* **1999**, *11*, 313.

(49) Sozzani, P.; Comotti, A.; Simonutti, R.; Meersmann, T.; Logan, J. W.; Pines, A. *Angew. Chem., Int. Ed.* **2000**, *39*, 2695.
(50) Comotti, A.; Bracco, S.; Valsesia, P.; Ferretti, L.; Sozzani, P. *J. Am. Chem. Soc.* **2007**, *129*, 8566.
(51) Cheng, C.-Y.; Bowers, C. R. *J. Am. Chem. Soc.* **2007**, *129*, 13997.
(52) Moudrakovski, I.; Soldatov, D. V.; Ripmeester, J. A.; Sears, D. N.; Jameson, C. J. *Proc. Natl. Acad. Sci. U.S.A.* **2004**, *101*, 17924.
(53) Cheng, C.-Y.; Stamatatos, T. C.; Christou, G.; Bowers, C. R. *J. Am. Chem. Soc.* **2010**, *132*, 5387.
(54) Böhlmann, W.; Pöppl, A.; Sabo, M.; Kaskel, S. *J. Phys. Chem. B* **2006**, *110*, 20177.
(55) Ueda, T.; Kurokawa, K.; Eguchi, T.; Kachi-Terajima, C.; Takamizawa, S. *J. Phys. Chem. C* **2007**, *111*, 1524.
(56) Ooms, K. J.; Wasylishen, R. E. *Microporous Mesoporous Mater.* **2007**, *103*, 341.
(57) Boutin, A.; Springuel-Huet, M.-A.; Nossov, A.; Gédéon, A.; Loiseau, T.; Volkringer, C.; Férey, G.; Coudert, F.-X.; Fuchs, A. H. *Angew. Chem., Int. Ed.* **2009**, *48*, 8314.
(58) Springuel-Huet, M.-A.; Nossov, A.; Adem, Z.; Guenneau, F.; Volkringer, C.; Loiseau, T.; Férey, G.; Gédéon, A. *J. Am. Chem. Soc.* **2010**, *132*, 11599.
(59) Kläui, W.; Schmidt, K.; Bockmann, A.; Hofmann, P.; Schmidt, H. R.; Stauffert, P. *J. Organomet. Chem.* **1985**, *286*, 407.
(60) Kepert, C. J. *Chem. Commun.* **2006**, 695.
(61) Kitaura, R.; Seki, K.; Akiyama, G.; Kitagawa, S. *Angew. Chem., Int. Ed.* **2003**, *42*, 428.
(62) Nelson, A. P.; Farha, O. K.; Mulfort, K. L.; Hupp, J. T. *J. Am. Chem. Soc.* **2009**, *131*, 458.
(63) Coombes, D. S.; Corà, F.; Mellot-Draznieks, C.; Bell, R. G. *J. Phys. Chem. C* **2009**, *113*, 544.
(64) Baumer, D.; Fink, A.; Brunner, E. *Z. Phys. Chem.* **2003**, *217*, 289.
(65) Raiford, D. S.; Fisk, C. L.; Becker, E. D. *Anal. Chem.* **1979**, *51*, 2050.
(66) van Geet, A. L. *Anal. Chem.* **1970**, *42*, 679.
(67) Cavanagh, J.; Fairbrother, W. J.; Palmer III, A. G.; Skelton, N. J. *Protein NMR Spectroscopy*; Academic Press: San Diego, CA, 1996; p 167.
(68) Huang, S. Y.; Anklin, C.; Walls, J. D.; Lin, Y.-Y. *J. Am. Chem. Soc.* **2004**, *126*, 15936.
(69) Findeisen, M.; Brand, T.; Berger, S. *Magn. Reson. Chem.* **2007**, *45*, 175.
(70) NIST webbook http://webbook.nist.gov/cgi/fluid.cgi?T=237&PLow=15&PHigh=20&PInc=&Applet=on&Digits=5&ID=C7440633&Action=Load&Type=IsoTherm&TUnit=K&PUnit=bar&DUnit=mol%2Fl&HUnit=kJ%2Fmol&WUnit=m%2Fs&VisUnit=uPa*s&STUnit=N%2Fm&RefState=DEF, 2010-12-14.
(71) Daan, F.; Smit, B., *Understanding Molecular Simulation: From Algorithms to Applications*; Academic Press: San Diego, CA, 1996; p 443.
(72) Assfour, B.; Seifert, G. *Int. J. Hydrogen Energy* **2009**, *34*, 8135.
(73) Rappé, A. K.; Casewit, C. J.; Colwell, K. S.; Goddard, W. A., III; Skiff, W. M. *J. Am. Chem. Soc.* **1992**, *114*, 10024.
(74) Bernardes, N. *Phys. Rev.* **1958**, *112*, 1534.
(75) Soler, J. M.; Artacho, E.; Gale, J. D.; García, A.; Junquera, J.; Ordejón, P.; Sánchez-Portal, D. *J. Phys. Condens. Mater.* **2002**, *14*, 2745.
(76) Ordejón, P.; Artacho, E.; Soler, J. M. *Phys. Rev. B* **1996**, *53*, 10441.
(77) Dion, M.; Rydberg, H.; Schröder, E.; Langreth, D. C.; Lundqvist, B. I. *Phys. Rev. Lett.* **2004**, *92*, 246401.
(78) Kong, L.; Román-Pérez, G.; Soler, J. M.; Langreth, D. C. *Phys. Rev. Lett.* **2009**, *103*, 096103.
(79) Jameson, C. J.; Jameson, A. K.; Cohen, S. M. *J. Chem. Phys.* **1973**, *59*, 4540.
(80) Sears, D. N.; Vukovic, L.; Jameson, C. J. *J. Chem. Phys.* **2006**, *125*, 114708.
(81) Khvostikova, O.; Assfour, B.; Seifert, G.; Hermann, H.; Horst, A.; Ehrenberg, H. *Int. J. Hydrogen Energy* **2010**, *35*, 11042.
(82) Assfour, B.; Seifert, G. *Microporous Mesoporous Mater.* **2010**, *133*, 59.
(83) Walker, A. M.; Civalleri, B.; Slater, B.; Mellot-Draznieks, C.; Corà, F.; Zicovich-Wilson, C. M.; Román-Pérez, G.; Soler, J. M.; Gale, J. D. *Angew. Chem., Int. Ed.* **2010**, *49*, 7501.
(84) Mulder, F. M.; Assfour, B.; Huot, J.; Dingemans, T. J.; Wagemaker, M.; Ramirez-Cuesta, A. J. *J. Phys. Chem. C* **2010**, *114*, 10648.
(85) Boutin, A.; Coudert, F.-X.; Springuel-Huet, M.-A.; Neimark, A. V.; Férey, G.; Fuchs, A. H. *J. Phys. Chem. C* **2010**, *114*, 22237.
(86) Neimark, A. V.; Coudert, F.-X.; Boutin, A.; Fuchs, A. H. *J. Phys. Chem. Lett.* **2010**, *1*, 445.
(87) Coudert, F.-X.; Jeffroy, M.; Fuchs, A. H.; Boutin, A.; Mellot-Draznieks, C. *J. Am. Chem. Soc.* **2008**, *130*, 14294.
(88) Coudert, F.-X.; Boutin, A.; Jeffroy, M.; Mellot-Draznieks, C.; Fuchs, A. H. *ChemPhysChem* **2011**, *12*, 247.
(89) Coudert, F.-X. *Phys. Chem. Chem. Phys.* **2010**, *12*, 10904.